Acta Cryst. (1998). D**54**, 922–937

X-ray Topographic Studies of Protein Crystal Perfection and Growth

I. Dobrianov,[a]* K. D. Finkelstein,[b] S. G. Lemay[a] and R. E. Thorne[a]

[a]*Laboratory of Atomic and Solid State Physics, Cornell University, Ithaca, NY 14853, USA, and* [b]*Cornell High-Energy Synchrotron Source (CHESS), Ithaca, NY 14853, USA. E-mail: ret6@cornell.edu*

(*Received 13 February 1997; accepted 4 March 1998*)

Abstract

The effects of solution variations during growth on the perfection of tetragonal lysozyme crystals have been characterized using X-ray topography and high angular and wavevector resolution reciprocal-space scans. X-ray images of crystals grown under nearly uniform conditions show little contrast or evidence of defects, and mosaic widths of these crystals are comparable with those reported for microgravity-grown crystals. Images of crystals for which solution conditions (temperature, pH or salt concentration) are changed after an initial period of uniform growth can show extensive contrast, indicating the presence of disorder. The X-ray mosaic widths of these crystals can be significantly broadened, but their radial widths are at most very slightly broadened, indicating that image contrast is primarily due to mosaicity. Comparison of X-ray images with mosaic scans indicates that regions grown after the change in solution conditions have broader mosaicities and are more disordered; that regions grown immediately after the change tend to have broader mosaicities than subsequent growth regions; and that the pre-change growth region is largely unaffected by solution changes. The observed disorder may arise from solution change-related transient growth instabilities, from transient liquid–liquid phase separation that can occur during the change, and from post-change relaxation of the lattice constant of the pre-change growth regions. These results suggest that solution variations during growth, including those typical of macroseeding, vapor-diffusion growth and other widely used techniques, may be an important source of disorder in some protein crystals.

1. Introduction

The most serious obstacle to determining the structure of proteins and other biological macromolecules by X-ray diffraction is the growth of crystals with suitable size and perfection (McPherson, Malkin & Kuznetsov, 1996; Rosenberger *et al.*, 1996; Durbin & Feher, 1996; Chayen *et al.*, 1996). Although protein crystals often have very small X-ray mosaic widths, they usually diffract to much lower resolution than inorganic crystals. The types of disorder that limit the diffraction resolution are in general not known. Protein crystal defects such as twins, inclusions, vacancies, dislocations, and incorporated crystalline and amorphous sediment have been observed using optical microscopy (Durbin & Feher, 1996), optical interferometry (Vekilov *et al.*, 1995; Kuznetsov *et al.*, 1995; Rosenberger *et al.*, 1996), atomic force microscopy (Durbin & Carlson, 1992; Konnert *et al.*, 1994; Malkin *et al.*, 1995; Yip & Ward, 1996), and most recently, X-ray topography (Fourme *et al.*, 1995; Stojanoff & Siddons, 1996; Izumi *et al.*, 1996; Stojanoff *et al.*, 1997). Real-time observations of growth using optical interferometry and atomic force microscopy (AFM) (Rosenberger *et al.*, 1996; Malkin *et al.*, 1995) have revealed mechanisms by which some of these defects form. The observed defects and defect-forming mechanisms largely parallel those of inorganic crystals (Chernov, 1997).

The only quantitative information about protein crystal defect densities has been provided by AFM measurements. Reported defect densities for canavalin, lysozyme, thaumatin and catalase are generally less than 10^5–10^6 cm^{-2} (Malkin *et al.*, 1995; McPherson, Malkin & Kuznetsov, 1996). Dislocation densities in canavalin crystals can be at the high end of this range but thaumatin, catalase and many lysozyme crystals show no evidence of dislocations. Densities of other kinds of defects have not been given, and the role of the interaction between the AFM tip and the soft surfaces of protein crystals in creating observed defects, particularly point defects like vacancies, has not been fully resolved. Notwithstanding these uncertainties, the observed defect densities lie within the normal range observed in inorganic crystals. For example, ordinary dislocation densities in metals range between 10^5 and 10^9 cm^{-2}, and cold worked metals can have dislocation densities as high as 10^{13} cm^{-2} (Newkirk & Wernick, 1962; Krivoglaz, 1996). Densities of point defects like vacancies and impurities routinely approach the lattice density (10^{15} cm^{-2}).

Are the defects and defect densities observed by AFM sufficient to account for the poor diffraction resolution of protein crystals? The fall-off of diffraction peak intensity with scattering angle is often characterized using the *B* factor (or 'thermal' factor), obtained by

fitting the envelope of the peak intensities using $I \propto \exp(-2B \sin^2\theta/\lambda^2)$. For inorganic crystals such as NbC, vacancy densities of several atomic percent (roughly 3×10^{13} cm^{-2}) produce attenuation of Bragg reflections with scattering angle corresponding to B factors of roughly 0.1 Å^2 (Krivoglaz, 1996; Metzger *et al.*, 1983; Webb, 1962). For protein crystals, B factors typically range between 5 and 100 Å^2. Vacancy densities per unit area required to produce a given B-factor scale as the fourth power of the lattice constant (Maimon, 1997). Thus, scaling by the lattice constant and B-factor ratios, the observed protein crystal B factors would require vacancy densities of at least several molecular percent, or roughly 10^9–10^{10} cm^{-2}. Required densities of other point defects like impurities and interstitials should be comparable. Similarly, in metals such as Ni, dislocation densities on the order of 10^{13} cm^{-2} produce attenuation of Bragg reflections corresponding to $B \simeq 0.1$ Å^2 (Koz'ma *et al.*, 1973). Crudely, the fall-off of Bragg peak intensity with scattering angle results from atomic or molecular displacements and molecular rotations within or at the boundary of a crystalline grain from the ideal periodic arrangement within that grain. Seemingly large defect densities produce relatively small B factors because for most defects the deviations from the local ideal periodic order are appreciable only within one or two lattice spacings of the defect.

Although a more rigorous analysis is needed, the above arguments suggest that the defects observed by AFM may not be sufficient to account for the limited diffraction resolution of many protein crystals. This is not necessarily surprising. Typical B factors obtained from protein structure refinements correspond (in a simple Debye–Waller analysis where $B = 8\pi^2\langle u^2\rangle$) to r.m.s. atomic displacements of 0.2–1.1 Å, or on the order of 1% of a lattice constant, and these could be produced by r.m.s. molecular rotations of a few degrees. At present, AFM can reliably resolve only relatively large displacements, such as those which occur at the cores of defects like vacancies and dislocations. The diffraction resolution may in most cases be limited by smaller displacements and rotations not associated with simple defects, by conformation variations, and perhaps by macromolecular impurities when present in the crystal at concentrations of several molecular percent.

Compared with inorganic crystals, protein crystals have some unusual properties that may be important in determining characteristic patterns of disorder and how they arise. The interactions between protein molecules are more complex, involving many non-specific interactions and perhaps only a few specific contacts, and these interactions can vary strongly with solution conditions. The conformation of a protein, and in particular of the surface groups involved in intermolecular contacts in a crystal, can vary from molecule to molecule and with solution conditions. The crystals contain substantial amounts of solvent, salt and other small molecules present in the mother liquor, and the concentrations and ordering of these can vary with solution conditions. As a result, protein crystals show extensive polymorphism, with some proteins crystallizing in more than a dozen forms. Furthermore, for a given polymorph, the lattice constants can vary by as much as several percent as solution conditions are changed. This behavior contrasts sharply with that of inorganic crystals, where molecular shape is fixed, polymorphism is relatively rare, lattice constants are independent of growth method, and lattice constant variations occur only due to thermal expansion, to the presence of impurities, or to external stresses.

The extra degrees of freedom possessed by protein crystals must lead to disorder, even at equilibrium in crystals grown under ideal conditions. For crystals grown under non-ideal conditions, the sensitivity of these degrees of freedom to solution conditions could be an important source of additional disorder. In the methods used for the vast majority of protein crystallizations (Ducruix & Giegé, 1992), solution conditions can vary substantially during the growth of an individual crystal. In vapor-diffusion growth, for example, the initial precipitant concentration in the well is typically twice that in the drop. The precipitant, protein and other solute concentrations in the drop thus can double during a crystallization experiment, producing significant changes in supersaturation, and drop pH can also change substantially (Rodeau *et al.*, 1991). Solution conditions can vary because the concentrations of protein and other solutes in the crystal are different than in the solution; growth leads to protein depletion and depletion or concentration of other solutes in the remaining solution (Elgersma *et al.*, 1992; Vekilov, Monaco *et al.*, 1996). Solution conditions can also vary because of the evolution of the patterns of convective and diffusive transport as the size of a crystal increases (Pusey *et al.*, 1988; Lin *et al.*, 1995).

We have investigated the effects of solution variations during and after growth on the perfection of tetragonal lysozyme crystals. X-ray topography and mosaicity measurements reveal characteristic patterns of disorder produced in response to solution changes. The disorder may arise from solution change-related transient growth instabilities, from incorporation of precipitate formed during the change, and from post-change relaxation of the lattice constant of the pre-change growth regions. Our results suggest that solution variations during growth may be an important source of disorder in many protein crystals.

2. Experimental methods

2.1. *Crystal growth*

Tetragonal hen egg-white lysozyme crystals were grown in acetate buffer at pH values near 4.5 using high-

Table 1. *Summary of typical growth conditions*

Growth parameters include the protein concentration c_p, NaCl concentration c_s, acetate buffer concentration c_{buffer}, pH and temperature T.

Growth type	C_p (mg ml^{-1})	c_s (M)	c_{buffer} (M)	pH	T (K)
Uniform	28	0.78	0.1	4.5	295
	61	0.45	0.1	4.5	295
ΔT (K)	28	0.78	0.1	4.5	295→288
ΔpH	34	0.75	0.1	5→4	295
$\Delta(c_s/c_p)$	61→11	0.45→1.2	0.2	4.5	295

purity commercial lysozyme (Seikagaku, 6× recrystallized) (Thomas *et al.*, 1996) and NaCl as the precipitant. Solutions were passed through 0.2 μm filters prior to use, and concentrations checked using refractometry. Supersaturations were estimated using the solubility data of Cacioppo & Pusey (1991). Hanging- and sitting-drop crystallization experiments employed siliconized cover slips and Q plates sealed using transparent tape. Experiments were set up using clean-room procedures in a HEPA-filtered laminar flow bench to reduce inhomogeneous nucleation.

Crystals were grown under both uniform and time-varying conditions. To obtain nearly uniform conditions, batch crystal growth was performed using 10–30 μl hanging drops. Well solutions having salt concentrations equal to that in the drops were added to minimize effects of water absorption by the polystyrene. Crystals for diffraction measurements were removed from drops containing at most a few crystals when they reached sizes on the order of 200–500 μm, to ensure that depletion of protein from the drop solution due to crystal growth was negligible (*i.e.* typically less than 5%, and at most 15% for the largest crystals in the 10 μl drops). Growth rates measured by optical microscopy were typically 10–20 μm h^{-1}.

To obtain time-varying growth conditions, crystals were grown in hanging drops under uniform conditions until they reached sizes on the order of 100–200 μm. The temperature, pH, salt concentration, or protein concentration was then changed, and further growth allowed under the new conditions. The growth temperature was changed by transferring the Q plate between room temperature and a custom thermoelectric incubator, giving a temperature equilibration time estimated to be less than 20 min. The growth solution pH was changed abruptly by physically transferring a crystal from one drop to a second drop having a different pH. The salt concentration was changed abruptly by transferring a crystal to a second drop with the same pH but a different salt concentration (and an appropriate well solution). The protein concentration was changed abruptly in a similar way. In the pH and salt concentration experiments, the protein concentration of the second drop was adjusted in each case to reduce the difference between initial and final growth rates. Crystals were transferred between drops in the liquid meniscus of a Pt wire loop. The time for the transfer was limited to a few s to minimize concentration changes due to evaporation, and care was taken so that the crystal did not touch the loop. For larger changes in salt concentration, small droplets of clouded solution formed when growth solution transferred with the crystal from the first drop mixed with the second growth solution, indicating that liquid–liquid phase separation occurred (Muschol & Rosenberg, 1997). The droplets formed immediately after the transfer, and dissipated within 15–30 min. To eliminate any effects of the phase separation, some crystals were prepared using a two-step transfer process: they were first 'rinsed' by transfer to a drop with intermediate protein and salt concentrations, and after 10–30 s were then transferred to the final drop for the remainder of the growth. This procedure eliminated visible clouding. No clouding was observed in any of the other growth experiments. Temperature stability during growth was typically ±0.5 K in ambient surroundings and ±0.05 K in the incubator.

Table 1 summarizes typical solution conditions used in the growth experiments. The changes explored were considerably larger than those that usually occur in lysozyme crystal growth. Lysozyme crystallizes easily throughout the range of conditions studied, and its structure is quite stable. Exaggerated changes in solution conditions were used to make observation of effects due to changes more likely, and to mimic the behavior of more sensitive proteins to changes more typical of standard growth methods.

Crystals for X-ray measurements were mounted in quartz capillaries, together with a small plug of mother liquor placed a few millimeters away. To minimize crystal temperature changes, capillaries were sealed using grease instead of wax and then transported to the X-ray source in multiwalled insulated containers. These procedures provided a temperature stability of ±2 K, comparable to temperature fluctuations at the synchrotron over the course of an experimental run. To reduce crystal strains and possible damage due to contact with the cover slips used in hanging-drop growth, only crystals on or near the surface of the drop were used. Many of these crystals are truncated from their ideal habit, due to proximity of one or more growth faces to the drop's surface.

2.2. *X-ray measurements*

Crystals were characterized primarily using X-ray topography, supplemented by $\theta - 2\theta$ and mosaic (ω) scans along and across the wavevector Q, respectively, of selected reflections. In X-ray topography (Barrett & Massalski, 1966; Tanner, 1976; Tanner & Bowen, 1980), the crystal is illuminated using a highly parallel X-ray beam. Under these conditions, the Bragg spots provide images of the crystal. Crudely, image contrast arises from variations in diffracted intensity at the selected

wavevector arising from variations in crystal lattice orientation and spacing (*i.e.* mosaic and strain) from point to point within the bulk of the crystal. Dynamical contrast mechanisms are likely to be less important than in metals and semiconductors, since protein crystals scatter weakly. The angular divergence of the incident beam determines the sensitivity to mosaic spread within the crystal and the lateral image resolution. X-ray topography has been used to image cracks, dislocations, and other defects in lysozyme crystals (Stojanoff & Siddons, 1996; Izumi *et al.*, 1996; Stojanoff *et al.*, 1997).

X-ray topographs were acquired at the Cornell High-Energy Synchrotron Source (CHESS) on bending magnet stations B-2 and C-2, using monochromatic 10 keV (1.24 Å) X-rays selected using Si [111] double-bounce monochromators. The X-ray beams energy spread at the sample was approximately 2 eV. The beam's vertical divergence $\Delta\varphi_v$ on both stations was approximately 4×10^{-5} rad (as determined by the synchrotron source size and the source-to-sample distance); the horizontal divergence $\Delta\varphi_h$ was roughly 5×10^{-4} rad on station B-2 and 1.6×10^{-4} rad on station C-2. These were calibrated by recording images of a 50 μm slit at different slit-to-film distances. The horizontal divergence was improved by a factor of eight in some measurements by inserting a horizontally diffracting Ge (220) channel-cut crystal upstream of the sample, but this reduced the X-ray flux at the sample by a comparable factor. These angular divergences resulted in an angular sensitivity (*i.e.* a sensitivity to crystal mosaic spread) ranging from ~0.002 to 0.03°. Because of the anisotropy between the horizontal and vertical beam divergences, topographs acquired using Bragg reflections lying within the vertical scattering plane had much greater sensitivity to lattice orientation variations than did those using Bragg spots lying in the horizontal plane. Thus, by selecting appropriate reflections, topographs providing images of crystal mosaicity with different sensitivities to mosaic spread could be obtained.

Diffraction patterns were recorded using Kodak Industrex SR film, held ~3 cm from the sample and perpendicular to the incident beam direction. Individual reflections were then optically magnified and digitally recorded. Exposure times ranged from 1 to 8 min without the Ge crystal, and 30–90 min with it. The angular beam divergence and sample-to-film distance gave a maximum lateral image resolution ranging from 2 to 15 μm. This was reduced slightly by the finite emulsion thickness (5 μm) and the non-normal incidence of the reflections on the film.

Lysozyme crystals were usually oriented with either the [001] axis or a ⟨110⟩ axis near the incident beam direction, and diffraction patterns recorded at several orientations over a range of several degrees. This typi-

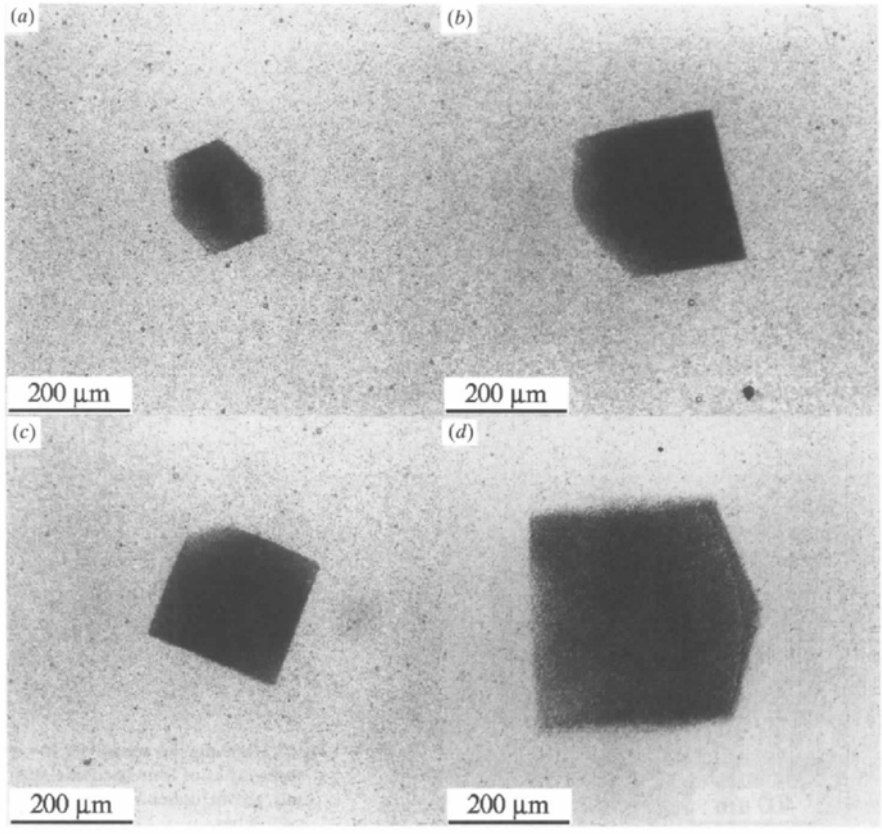

Fig. 1. Low angular sensitivity X-ray topographs of four lysozyme crystals grown under nearly uniform conditions.

cally yielded between 10 and 30 Bragg reflections for each crystal that provided useable images. No image degradation due to radiation damage was observed in any of the measurements. As is apparent from previous work, X-ray topography is extremely sensitive to certain kinds of lattice disorder, but identifying the kinds of disorder responsible for observed contrast patterns can be difficult. Image contrast varies from reflection to reflection (since each probes a different Fourier component of the lattice) and for different crystal orientations within a given reflection. Some contrast may reflect the pathologies of particular crystals, such as those whose defect structures are established by errors in the initial stages of crystallization, or that are damaged by post-growth handling. The results presented here are representative of general trends and characteristic contrast patterns observed in measurements of more than 3000 reflections from more than 160 crystals.

To further characterize the crystals and assist in the interpretation of the topographs, high-resolution mosaic (ω) and $\theta - 2\theta$ scans through selected reflections were performed on CHESS station C-2 using a Huber six-circle diffractometer and Si (111) monochromator and analyzer crystals. Mosaic scans across the wavevector were performed by rotating the crystal about an axis perpendicular to the scattering plane defined by the incident and reflected wave vectors while keeping the detector fixed, and measured the distribution of lattice orientations within the crystal. Radial scans along the wavevector were performed by rotating the crystal and detector arm together by angles of θ and 2θ, respectively, and measured the distribution of Bragg plane spacings within the crystal. Most scans were performed at a detector angle $2\theta \simeq 23°$, roughly matching the Bragg angles of the Si monochromator and analyzer crystals and corresponding to a Bragg plane spacing $d \simeq 3.6$ Å. The instrumental resolutions for the two types of scans were $(\Delta\theta)_{IR} \simeq 0.003°$ and $\Delta Q/Q \simeq 1.4 \times 10^{-4}$ or $\Delta(2\theta)_{IR} \simeq 0.003°$ at $2\theta \simeq 23°$, respectively.

3. Experimental results

3.1. *Effect of growth under nearly uniform conditions*

Figs. 1 and 2 show topographs of eight lysozyme crystals grown under nearly uniform conditions. The images are negatives, so that strongly diffracting regions appear darker. The images in Fig. 1 were obtained from reflections near the horizontal scattering plane, and thus have relatively low angular sensitivity (>0.01°). Under these conditions, uniform growth crystals usually show no contrast. For some crystals, thinning due to growth truncation by the drop's surface produces gradual

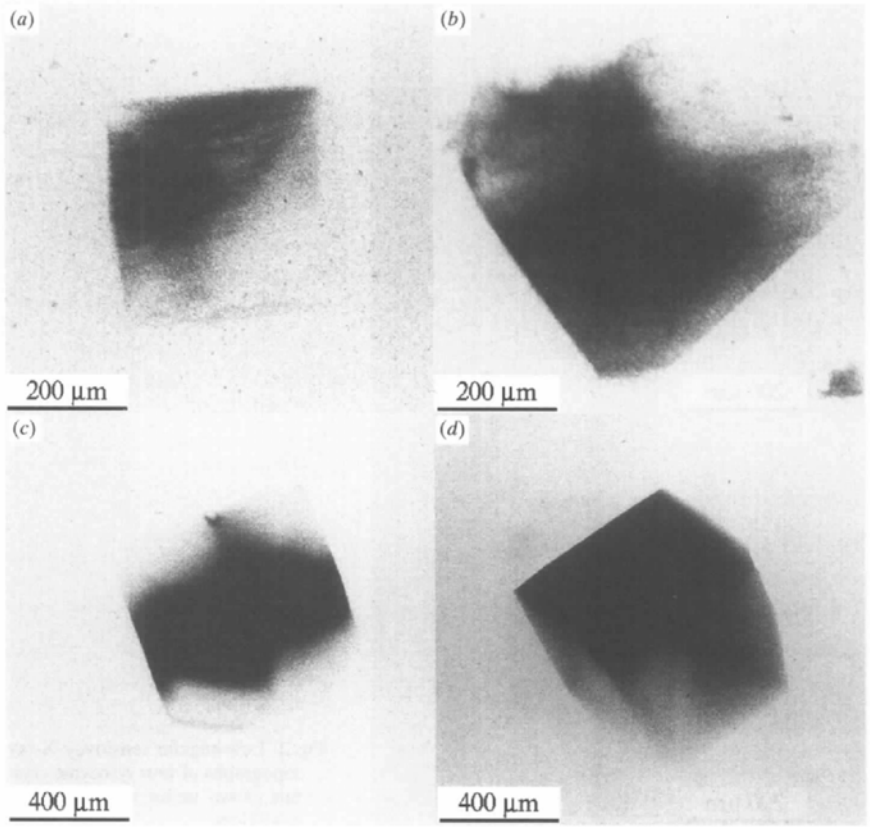

Fig. 2. High angular sensitivity X-ray topographs of four lysozyme crystals grown under nearly uniform conditions.

intensity variations, as in Fig. 1(*b*). Occasionally, the images showed horizontal striations similar to those reported previously (Izumi *et al.*, 1996; Stojanoff *et al.*, 1997). These striations always ran parallel to the horizontal scattering plane, regardless of crystal orientation and habit, and are likely to be a result of variations in the thickness of the X-ray beamline's Be window (Cloeten *et al.*, 1996; Long, 1998).

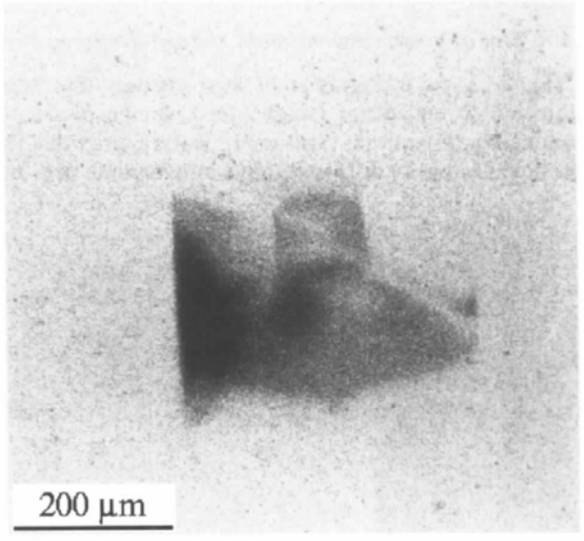

Fig. 3. High angular sensitivity topograph of a lysozyme crystal subjected to a 7 K temperature change during growth. The interior boundary visible in the topograph corresponds to the crystal boundary when the temperature was changed.

Fig. 2 shows high angular sensitivity (<0.005°) images of four uniform growth crystals obtained from reflections near the vertical scattering plane. In this case, the diffracted intensity varies smoothly on a scale smaller than but comparable to the crystal dimensions, indicating that the orientation and/or spacing of the crystal lattice varies slightly on this scale. Some more abrupt contrast variation is evident in (*a*) and (*d*), and this is most likely to be associated with sectoriality (Chernov, 1997). The absence of any other sharp boundaries suggests that the observed contrast is dominated by a more or less continuous change in the lattice. Sharp contrast that would indicate the presence of dislocations or other defects is also largely absent.

3.2. *Effect of a temperature change during growth*

Fig. 3 shows a high angular sensitivity topograph of a crystal that was subjected to a temperature change of 280 K during growth. The image shows a difference in diffracted intensity between the pre-change and post-change growth regions, but no evidence for dislocations or other defects. The symmetry of the pattern suggests

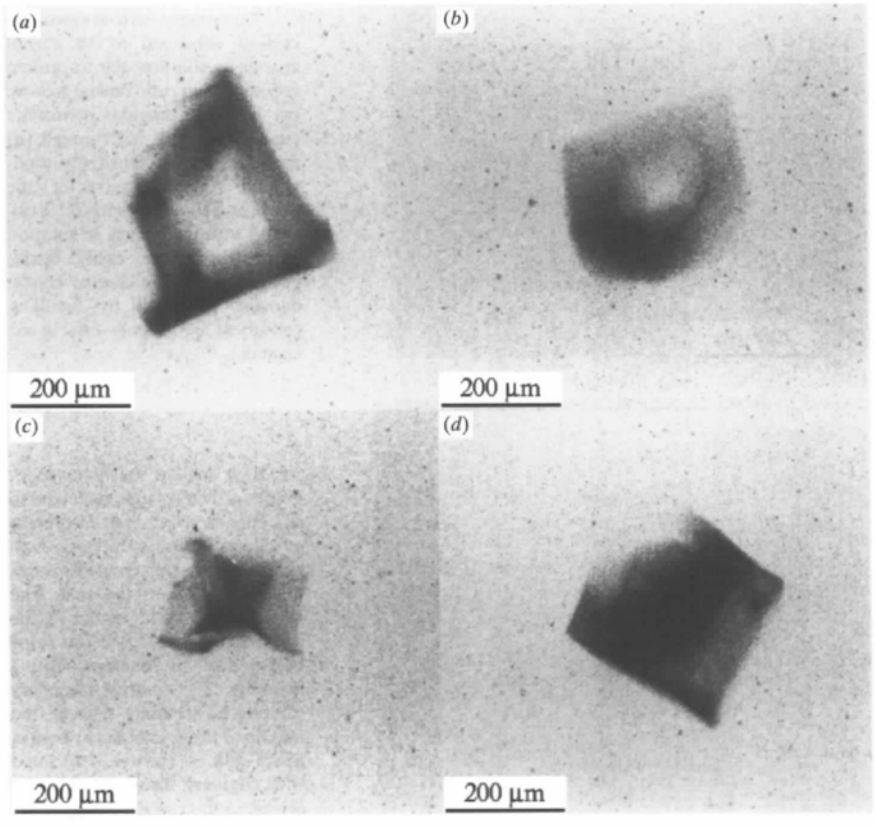

Fig. 4. Topographs of four lysozyme crystals subjected to an abrupt change in solution pH from 4 to 5 during growth; (*a*) and (*b*) are low angular sensitivity topographs, while (*c*) and (*d*) are high angular sensitivity topographs. The patterns observed and, in particular, the sharpness of the boundary between pre- and post-change growth regions depends upon the reflection studied, because each reflection 'views' the crystal in a different orientation, and because the crystal has a finite thickness along the incident beam direction.

that the contrast is due to a difference in either the lattice mosaicity or lattice constant. Topographs of crystals subjected to smaller temperature changes show less contrast.

3.3. *Effect of a pH change during growth*

Fig. 4 shows topographs of four crystals that were subjected to an abrupt change in solution pH from 4 to 5 during growth. The diffracted intensity differs significantly between the pre-change and post-change growth regions, even in the low angular sensitivity images (*a*) and (*b*). The intensity within the pre-change growth region tends to be quite uniform. Intensity variations are occasionally observed in the post-change region, including sharp linear features consistent with dislocations.

3.4. *Effect of a salt concentration change during growth*

Fig. 5 shows topographs of four crystals that were subjected to an abrupt (single-step) change in salt-to-protein concentration ratio c_s/c_p during growth. The diffracted intensity differs strongly between the pre- and

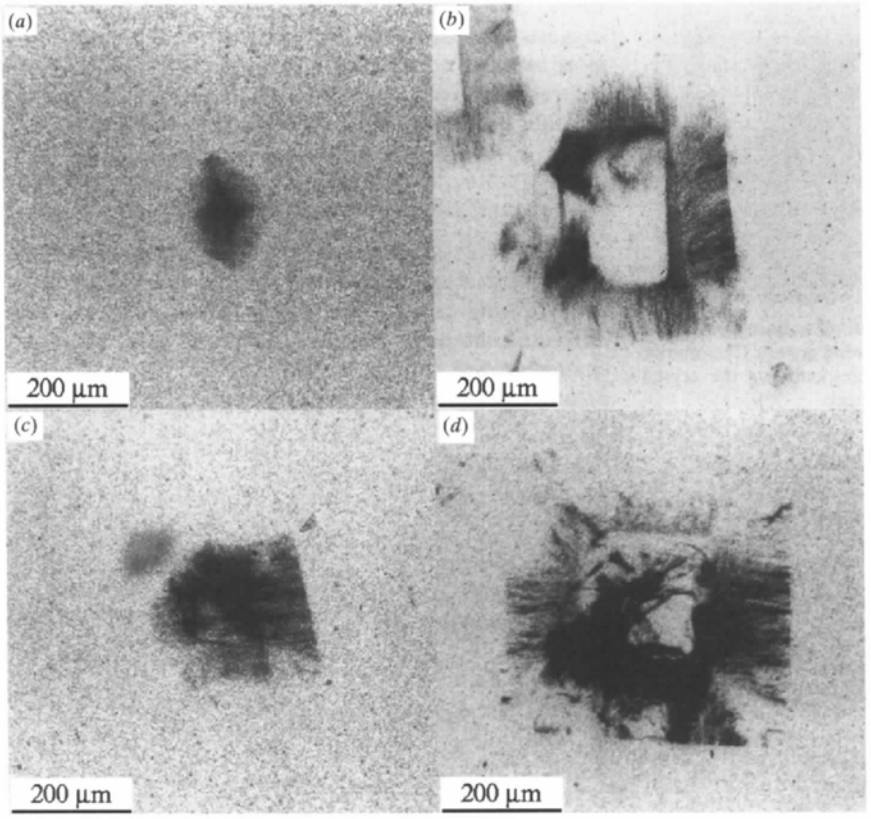

Fig. 5. Topographs of four lysozyme crystals subjected to an abrupt change in solution salt-to-protein concentration ratio during growth; (*a*) is a low angular sensitivity topograph, while (*b*) through (*d*) are high angular sensitivity topographs. The symmetry of the patterns allows contrast associated with the change in solution conditions to be easily distinguished from that due to crystal damage produced by handling (observed in roughly one in six crystals).

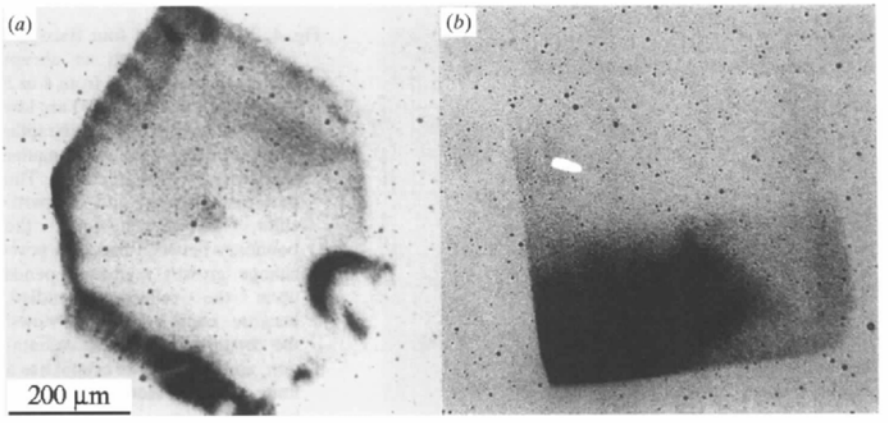

Fig. 6. High angular sensitivity topographs of two crystals subjected to a change in salt-to-protein concentration ratio during growth using the two-step transfer procedure discussed in the text. The semi-circular band visible in the lower right of the crystal in (*a*) is likely due to damage during handling. The contrast boundary running horizontally through the middle of the crystal in (*b*) is most likely due to stresses associated with capillary forces holding the crystal to the capillary wall.

post-change growth regions in both high and low angular sensitivity images, indicating a significant difference in lattice mosaicity or lattice constant between these regions. The diffracted intensity from the post-change growth regions shows pronounced variations indicating the presence of significant disorder, whereas the intensity from the pre-change growth region tends to be uniform. Many images show sharp lines in the post-change region, indicating the presence of dislocations. In Figs. 5(*b*)–5(*d*), arrays of dislocation lines radiate from the boundary outward into the post-change growth region. The lines tend to propagate along ⟨110⟩ directions, as indicated by their normal orientation to the boundary and by their absence from the corners of the post-change growth region.

The concentration changes for the crystals of Fig. 5 were sufficient to cause cloudy droplets to form in the immediate vicinity of the crystal after the transfer to the final growth solution, indicating the presence of liquid–liquid phase separation. These droplets disappeared within 15–30 min after the transfer. Fig. 6 shows high-angular sensitivity topographs of two crystals subjected to a similar change in c_s/c_p using a two-step procedure that did not produce visible clouding. In this case, the density of dislocation lines radiating from the boundary between pre- and post-change growth regions is greatly reduced. The topographs more closely resemble those obtained for crystals subjected to a change in pH, and low angular sensitivity topographs show little contrast. This suggests that the dislocation lines evident in Figs. 5(*b*)–5(*d*) are primarily a consequence of liquid–liquid phase separation in the growth solution.

Fig. 7 compares pre- and post-change optical images with a topograph of a crystal subjected to a change in c_s/c_p using the one-step procedure. Many features visible in the topographs have signatures in the optical images, presumably because changes in crystalline order produce small changes in density, solvent content, and refractive index. For example, the boundary at which solution conditions were changed appears as a striation or veil in the optical image. Similar veils are often observed in the general practice of protein crystal growth, particularly in seed-grown crystals. Monaco & Rosenberger (1993) have extensively discussed veils in lysozyme crystals produced in response to changes in temperature during growth. The correspondence between the X-ray and optical images indicates that optical techniques such as interference microscopy and laser scattering tomography should be useful in observing protein crystal disorder, although the information provided will be more limited than that available using X-ray techniques.

3.5. *Effect of a protein concentration change during growth*

To investigate the effects of changes in protein concentration, crystals were transferred mid-way during growth to a second solution differing only in protein concentration. The accessible concentrations were constrained by an absence of nucleation at lower concentrations and excessive nucleation and growth rates at higher concentrations. For crystals subjected to a concentration change of 50% from 27 to 41 mg ml^{-1},

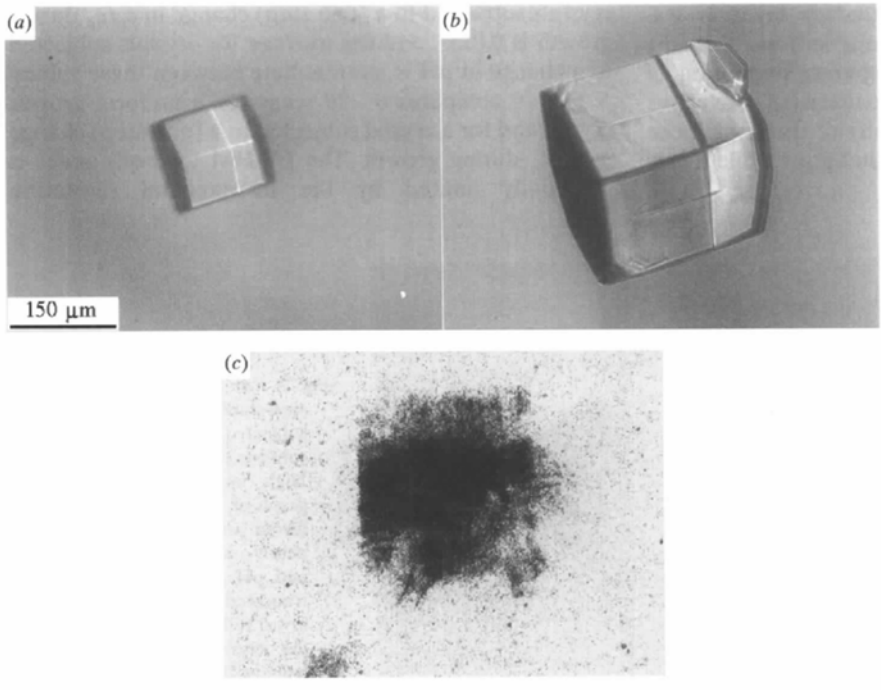

Fig. 7. Comparison of optical images with a topograph of a lysozyme crystal subjected to an abrupt change in solution salt-to-protein concentration ratio during growth. The optical image in (*a*) was taken just after the change in solution, and the image in (*b*) was taken when growth was completed. Many of the features visible in the topograph have signatures in the optical image.

which produced a factor-of-three change in growth rate, high angular sensitivity topographs are essentially featureless, except in the immediate vicinity of the pre-transfer crystal boundary as discussed in §3.6. Topographs of crystals grown for extended periods in small-volume drops so as to produce substantial protein depletion are also essentially featureless. This suggests that the contrast observed for crystals subjected to changes in temperature, pH, and salt concentration is not due to changes in protein concentration or growth rate.

3.6. *Effect of transient solution conditions*

Fig. 8(*a*) shows a low angular sensitivity topograph of a crystal subjected to a change in pH during growth. The scattered intensity from the boundary layer just outside the pre-change growth region differs strongly from earlier and subsequent growth regions. This suggests that crystal layers that grow immediately after the change in conditions are more disordered than those that grow before, and that crystal perfection recovers somewhat in subsequent growth layers. Similar behavior was observed for crystals subjected to a change in salt concentration. Fig. 8(*b*) shows a high angular sensitivity topograph of a crystal that was grown under uniform conditions in one drop and then transferred to a second drop having the same solution concentrations for further growth. The scattered intensity from the boundary region again differs from that of the pre- and post-transfer growth regions on either side of it, which in this case have roughly equal intensity. Low angular sensitivity topographs of this crystal appear completely uniform, indicating that the boundary layer is less disordered than in (*a*). These results indicate that any change in solution conditions, including disruption of the concentration profiles and the patterns of convective and diffusive transport in the vicinity of the crystal, can produce excess disorder in layers that grow while a new steady state is being established.

3.7. *Reciprocal-space scans*

To characterize crystal mosaicity and strains and to assist in the interpretation of topographs, high-resolution reciprocal space scans across and along the scattering wavevector were performed on several crystals, using reflections in the vertical scattering plane. Crystals with gross imperfections arising from growth accidents or damage during handling were screened out using topography.

Fig. 9 compares mosaic (ω) scans for a uniform growth crystal and for a crystal subjected to an abrupt change in c_s/c_p during growth (using a one-step transfer as for the crystals of Fig. 5). The peak full width at half maximum (FWHM) for the non-uniform growth crystal is considerably larger than that for the uniform growth crystal (0.013 *versus* 0.0051°), and the diffracted intensity in the wings of the peak falls off much more gradually. For the uniform growth crystal, the intensity falls to background within roughly 2 FWHM's of the peak, as would be expected for a Gaussian mosaic distribution. For the nonuniform growth crystal, appreciable intensity was observed several tenths of a degree from the peak, indicating a highly non-Gaussian mosaic.

Table 2 summarizes the FWHM values and mosaic widths η {obtained by correcting the FWHM for the instrumental resolution using $\eta = [(\text{FWHM})^2 - (\Delta\theta_{IR})2]^{1/2}$} for several crystals. The average FWHM value and mosaic width for the uniform growth crystals are 0.0047 and 0.0037°, respectively, which compare favorably to an average rocking width of 0.0047° reported by Snell *et al.* (1995) for tetragonal lysozyme crystals grown in microgravity using acetate buffer and NaCl as the precipitant. The average mosaic width for crystals subjected to a (one-step) change in c_s/c_p during growth is 0.015°, and the average for crystals subjected to a change in pH is intermediate between these values.

Fig. 10 compares $\theta - 2\theta$ scans for a uniform growth crystal and for a crystal subjected to a (one-step) change in c_s/c_p during growth. The FWHM for both peaks is essentially limited by the instrumental resolution

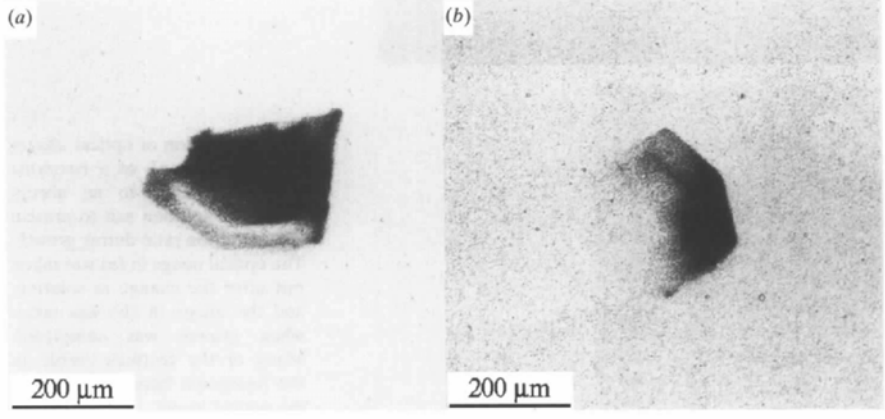

Fig. 8. (*a*) Low angular sensitivity topograph of a lysozyme crystal subjected to an abrupt change in solution pH during its growth. (*b*) High angular sensitivity topograph of a crystal that was transferred to a new solution with nearly identical concentrations and pH during its growth. The truncated form of the topograph in (*a*) reflects the actual shape of the crystal that resulted from hanging-drop growth.

$\Delta(2\theta)_{IR} \simeq 0.003°$, and any difference in width is less than the observed sample-to-sample variations (~0.002°). The observed peak widths imply that the distributions of Bragg plane spacings within the crystals have fractional widths of less than 0.02%, and that the crystals are not, on average, appreciably strained.

These results do not rule out the presence of substantial strains within a small fraction of the crystal volume, such as in the vicinity of dislocations, since these would contribute only to the poorly resolved wings of the peaks and to diffuse scattering. It is worth noting that even a small volume fraction containing large strains is sufficient to produce large mosaicity. For example, in a crystal comprised of a few macroscopic grains with each having a different lattice orientation, large strains need only occur in the immediate vicinity of the grain boundaries. Furthermore, even very small strains can produce significant mosaicity in sufficiently large crystals. An average strain due to bending of only ~0.01% could give a mosaicity of ~0.01° in a 1 mm crystal.

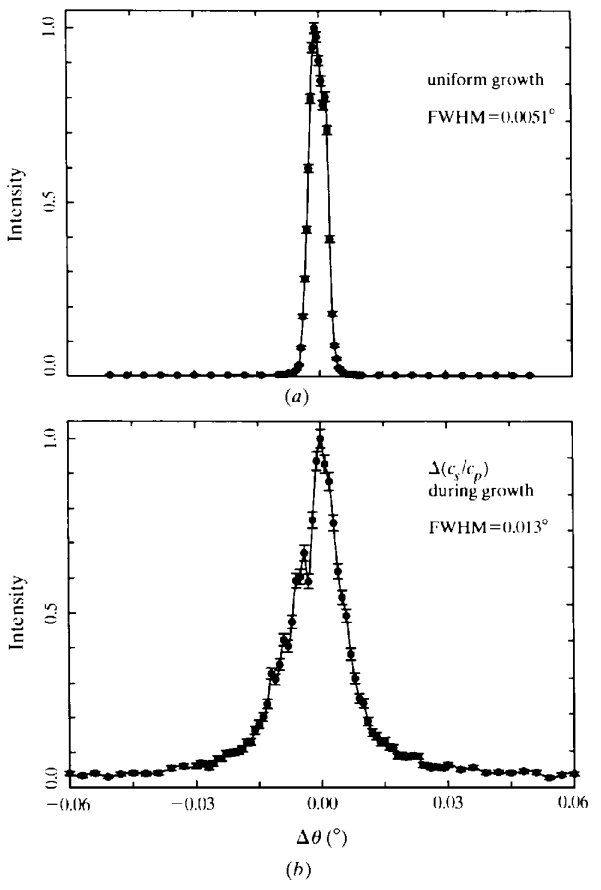

Fig. 9. Mosaic (ω) scans across the diffracting wavevector for (a) a lysozyme crystal grown under uniform conditions, and (b) a crystal subjected to an abrupt change in solution salt-to-protein concentration ratio during growth. The reflections have $2\theta \simeq 23°$ and the instrumental resolution is $(\Delta\theta)_{IR} \simeq 0.003°$.

Table 2. *Summary of mosaic scan FWHM's and corresponding mosaic widths [corrected for the instrumental resolution $(\Delta\theta)_{IR} \simeq 0.003°$]*

Crystal type	Crystal No.	FWHM (°)	Mosaic width (°)
Uniform growth			
	1	0.0050	0.0040
	2	0.0037	0.0022
	3	0.0038	0.0023
	4	0.0063	0.0055
ΔpH during growth			
	1	0.0083	0.0077
	2	0.0061	0.0053
$\Delta(c_s/c_p)$ during growth			
	1	0.013	0.013
	2	0.013	0.013
	3	0.011	0.011
	4	0.022	0.022
	5	0.016	0.016

3.8. *Relation between topographic contrast and mosaicity*

The very small radial widths and broadenings of the diffraction peaks in Fig. 10 imply that the contrast observed in topographs must primarily be due to lattice mosaicity (although strain may produce additional contrast in the vicinity of defects like dislocations). Consequently, topographs acquired at successive angles within the mosaic width of a diffraction peak can be used to map out the mosaicity of each part of the crystal, and the contribution of each part to the observed mosaic curve.

Fig. 11 shows a series of high angular sensitivity topographs acquired as a crystal grown under uniform conditions was rocked in 0.01° steps through its mosaic curve. Different macroscopic regions of the crystal diffract most strongly at each orientation, in a way that suggests the presence of a gradual bending of the lattice. These results differ from those of Fourme *et al.* (1995), who studied a lysozyme crystal with three distinct peaks in its mosaic curve, the found using topography that discrete macroscopic mosaic blocks diffracted strongly in each peak.

Fig. 12 shows a series of high angular sensitivity topographs acquired as a crystal subjected to an abrupt (single-step) change in c_s/c_p during growth was rocked in 0.01° steps through its mosaic curve. In (a) (the orientation that yielded the largest overall diffracted intensity), the pre-change growth region diffracts strongly. As the crystal is rocked off the peak, diffraction from this region falls off rapidly, and is very weak at $\Delta\theta = 0.02°$. In contrast, diffraction from the post-change growth region falls off much more gradually. At $\Delta\theta = 0.05°$, strong diffraction is still observed from the dislocation lines and from the narrow growth band adjacent to the pre-change growth region. These images suggest that the pre-change growth region has a small mosaicity and is relatively well ordered, whereas the post-change growth region has a broader mosaicity and is relatively disordered. The most heavily disordered regions are

those just outside the pre-change growth region and in the vicinity of the dislocation lines.

4. Discussion

4.1. *Interpreting image contrast: macroscopic versus microscopic mosaicity*

Mosaicity measurements have been used as a supplement to diffraction resolution measurements for characterizing protein crystal perfection (Shaikevitch & Kam, 1981; Helliwell, 1988; Snell *et al.*, 1995; Fourme *et al.*, 1995; Chayen *et al.*, 1996; Snell, 1997; Otalora *et al.*, 1997). To understand how mosaicity produces image contrast in topographs and how this contrast is related to lattice disorder, it is useful to make a distinction between 'macroscopic' mosaicity and 'microscopic' mosaicity, as schematically illustrated in Fig. 13.

In a crystal with macroscopic mosaicity, the characteristic length scale on which the lattice orientation varies is smaller than but on the order of the crystal dimensions, such as in a crystal that contains a few twin or small-angle grain boundaries or that is weakly strained. The local lattice order (which controls the fall-off of diffracted intensity with scattering angle) may be essentially perfect except in small volumes bordering grain boundaries. Consequently, a crystal with macroscopic mosaicity may have a large mosaic spread even

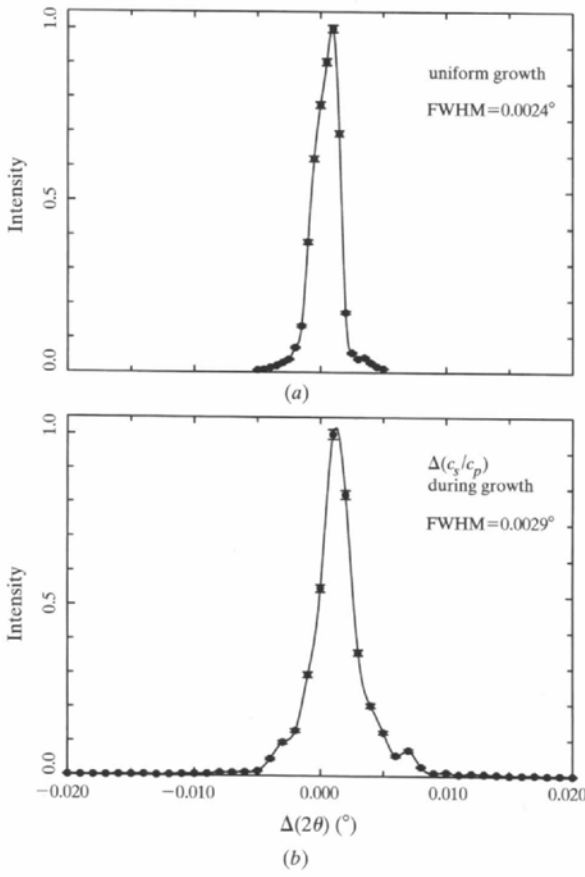

Fig. 10. Radial (θ–2θ) scans along the diffracting wavevector for (*a*) a lysozyme crystal grown under uniform conditions, and (*b*) a crystal subjected to an abrupt change in solution salt-to-protein concentration ratio during growth. The reflections have $2\theta \simeq 23°$ and the instrumental resolution is $\Delta(2\theta)_{IR} \simeq 0.003°$.

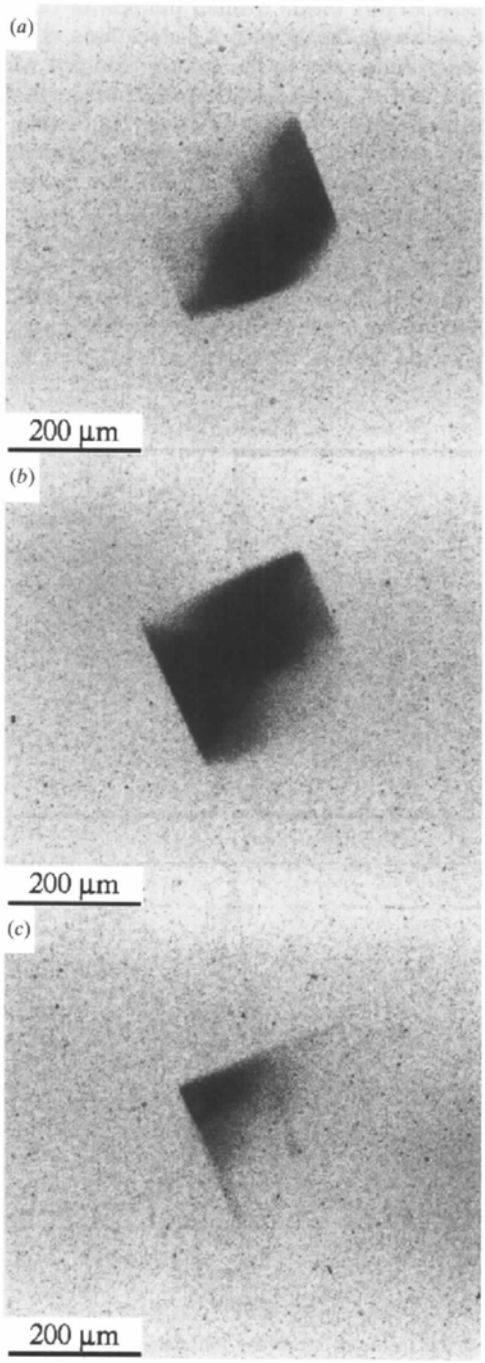

Fig. 11. High angular sensitivity X-ray topographs of a lysozyme crystal grown under uniform conditions, acquired at 0.01° intervals in the rocking curve of the reflection.

though it is microscopically well ordered, has a small B factor and diffracts to high resolution. For example, cryocooling often broadens the mosaic width by a factor of ten or more to several tenths of a degree, and yet the diffraction resolution often improves. The mosaic likely broadens because macroscopic grains with slightly different orientations are formed when the crystal cracks during cooling, and the resolution improves because the microscopic lattice disorder within the grains is reduced.

In a crystal with microscopic mosaicity, the lattice orientation varies on a much shorter length scale. Microscopic mosaicity may be directly or indirectly connected to the B factor and diffraction resolution. If the microscopic disorder present in the crystal consists only of modulations of the local lattice orientation, then the extent of the disorder will be determined by the magnitude and the correlation length of these modulations. For lattice bending on the length scale a of the unit cell, the diffraction resolution d for a given mosaic width η is of the order ηa (Shaikevitch & Kam, 1981). For $d \simeq 2$ Å and $a \simeq 50$ Å, this implies a mosaic width of a few degrees, much larger than what is usually observed, and bending on longer length scales would require even larger mosaic widths to achieve a given d. A more likely possibility is that the B factor and diffraction resolution

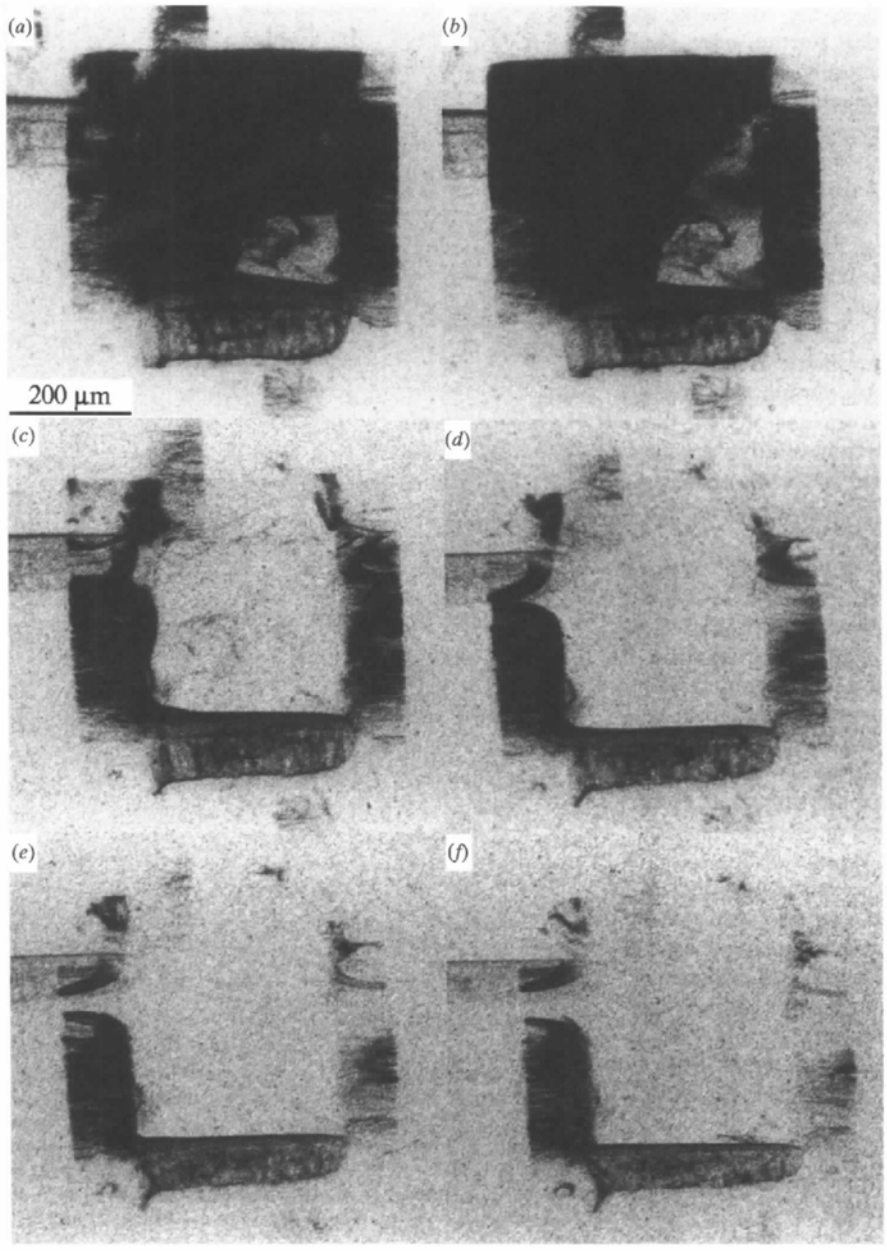

Fig. 12. High angular sensitivity topographs of a lysozyme crystal subjected to an abrupt change in solution salt-to-protein concentration ratio during growth, acquired at 0.01° intervals in the rocking curve of the reflection beginning in (*a*) near the reflection's peak.

are dominated by molecular displacements, rotations and conformation variations. In this case, mosaicity may be produced by the random accumulation of these unit-cell scale 'errors'. Since lattice orientation variations are then only a symptom of the disorder that limits the B factor and diffraction resolution, the mosaicity associated with a given diffraction resolution may be very small.

In evaluating crystals for use in protein structure determinations, microscopic mosaicity is more important since it can be related to the disorder that produces the decrease in diffracted intensity with scattering angle. Macroscopic mosaicity appreciably affects the overall signal-to-noise ratio only when the illuminating X-rays have low angular divergence, unless the mosaicity is large enough to produce spot overlap. Furthermore, the mosaicity usually broadens substantially when crystals are frozen for data collection or subjected to other post-growth treatments, so that the as-grown macroscopic mosaic width seldom dominates. Since mosaic scans like those shown in Fig. 9 cannot easily distinguish between microscopic and macroscopic mosaicity, they are of limited use in characterizing protein crystal perfection.

X-ray topography is a more useful characterization tool because it allows these two kinds of mosaicity to be distinguished. For a crystal with large macroscopic mosaicity and small microscopic mosaicity, as shown in Fig. 13(a), high angular sensitivity topographs will show strong diffracted intensity only from regions of the crystal having appropriate orientation relative to the incident X-ray beam. As the crystal is rocked through the mosaic curve of the reflection, different regions will light up and then fade.

For a crystal having only uniform microscopic mosaicity, topographs will show little or no contrast (aside from that due to variations in crystal thickness), since the length scale of the orientation variations is comparable to or smaller than the lateral image resolution. For a crystal having microscopic mosaicity whose width varies from region to region, topographs will show contrast that depends upon the orientation of the crystal and the relative mosaic widths of each region. As an example, consider a crystal having a narrow mosaic width region surrounded by a wide mosaic width region, as shown in Fig. 13(b). When the crystal is oriented at the peak of its overall mosaic curve, the diffracted intensity from the middle region will be stronger than from the outer region, and the topograph will appear as a light ring with a dark hole. When the crystal is rocked off the peak, the diffraction from the narrow-width region will fade faster, and eventually an inverted image consisting of a dark ring and a light hole will be obtained.

For uniform growth crystals, the contrast observed in Figs. 1, 2 and 11 suggests the presence of macroscopic mosaicity with a small width (perhaps associated with stresses due to capillary forces holding the crystal to the capillary wall). The microscopic mosaic has an even smaller width, but estimating its width is difficult because the incident beam divergence (0.003°) is less than a factor of two smaller than the full mosaic width of typical crystals.

For crystals subjected to changes in pH and salt concentration during growth, the observed contrast is determined partly or largely by microscopic mosaicity.

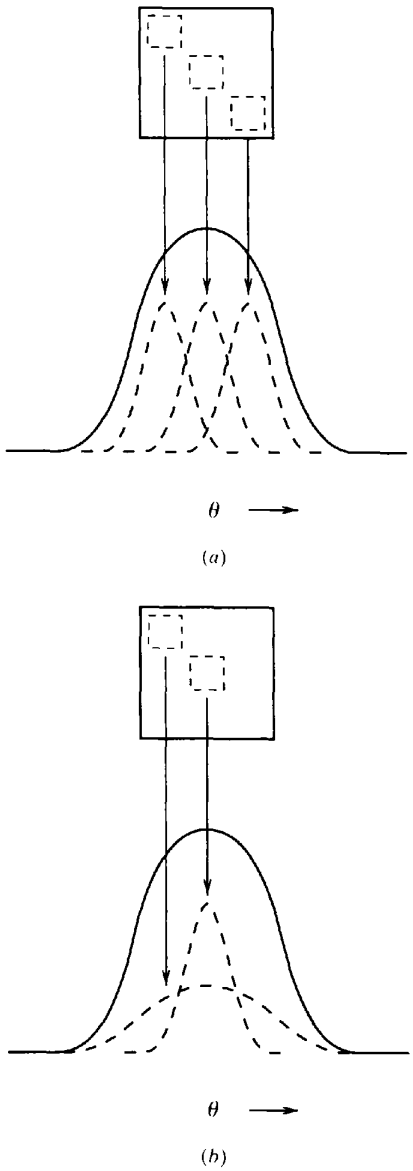

Fig. 13. Schematic illustration of the difference between macroscopic and microscopic mosaicity. In (a), different regions of the crystal diffract over a comparable range of angles (*i.e.* they have comparable microscopic mosaicities), but each diffracts most strongly at a different angle, producing a broad overall mosaic curve. In (b), different regions of the crystal diffract most strongly at the same angle, but the range of angles over which each diffracts varies.

This is particularly clear in Fig. 12, which indicates that the microscopic mosaicity of the pre-change growth region is smaller than that of the post-change region. The regions just outside the pre-change growth region and in the vicinity of dislocation lines have the largest mosaicity, and are responsible for the broad, non-Gaussian wings of the mosaic curve in Fig. 9(*b*). These conclusions can also be reached by examining different reflections acquired at a single orientation of this crystal. The majority of the reflections show a light pre-change growth region and a darker post-change growth region. The crystal orientation is random relative to the peak of each reflections rocking curve, and so regions with broader mosaicities appear darker in more reflections.

4.2. *Origin of the disorder*

Most lysozyme crystals grown under uniform conditions yield essentially featureless topographs, and usually show no evidence of dislocations or other extended defects, of solvent inclusions, or of included crystallites. One possible explanation is that such defects may not be detectable, either because they are too small to be resolved or because their effects on diffraction are too weak. A more likely explanation may be that the crystals are in fact nearly free of these defects. Electron-microscopy studies on tetragonal lysozyme (Durbin & Feher, 1990) observed only occasional growth spirals associated with screw dislocations and no evidence of inclusions. AFM studies (Durbin *et al.*, 1993; Malkin *et al.*, 1995) observed growth spirals only for crystals grown at low supersaturations, and growth by two-dimensional nucleation with no evidence of dislocations at higher supersaturations more typical of growth experiments. The present results, obtained using a bulk rather than surface-sensitive technique, support the conclusion that densities of inclusions and dislocations in lysozyme crystals can be very low. Etching experiments (Monaco & Rosenberger, 1993) suggested much higher defect densities, but these may have been an artefact of the growth method used.

Crystals subjected to changes in solution conditions during growth show increased disorder in the post-change growth region. How do solution changes give rise to this disorder? There are several possibilities. First, solution changes may produce changes in growth kinetics that lead to disorder. For example, surface nucleation rates, step velocities, and growth rates may fluctuate as concentration and flow profiles adjust to a new steady state, leading to enhanced incorporation of impurities and other foreign particles and to step bunching and other instabilities that produce disorder (Tiller, 1991; Monaco & Rosenberger, 1993; Vekilov, Monaco *et al.*, 1996; Vekilov, Alexander *et al.*, 1996; Chernov & Komatsu, 1995; Chernov, 1997). In the present experiments, the increased mosaicity of growth layers immediately adjacent to the pre-change growth region, even in crystals transferred to an identical growth solution, provides clear evidence that fluctuations in growth kinetics can lead to disorder.

A second possibility is that changes in solution conditions may lead to formation of precipitate, microcrystals, or protein-rich droplets which when incorporated into the growing crystal lead to formation of inclusions (Tiller, 1991; Chernov & Komatsu, 1995; Chernov, 1997). Mistakes when the lattice is closed around the inclusions could then generate dislocations. Patterns of disorder strikingly similar to that shown in Figs. 5 and 12 have been observed in seed-grown crystals of a variety of materials including $NH_4H_3(C_2O_4)_2{\cdot}2H_2O$, triglycine sulfate, KDP, thiourea and natural quartz (Klapper, 1980). In these systems, inclusions are formed due to irregularities on the surface of the seed and due to fluctuations in supersaturation and flow patterns. These inclusions nucleate dislocations which tend to propagate outward in particular directions determined by the elastic anisotropy of the crystal and the Burgers vector of the dislocation. In the present experiments, changes in growth conditions that lead to transient liquid–liquid phase separation (*i.e.* single-step changes in c_s/c_p) yield by far the largest dislocation densities in the post-change growth region. Most of these dislocations appear to originate just outside the pre-change growth boundary, consistent with disappearance of the cloudy droplets within 30 min, or after less than ~10 μm of post-change growth.

A third possibility is that the shock of the change in solution conditions may cause the pre-change growth region to become disordered. This disorder may then propagate out into subsequent growth layers. However, the topographs in Fig. 12 show that the pre-change growth region has a smaller mosaicity than the post-change region. Furthermore, crystals that are soaked after growth in a solution with a much different salt concentration than their mother liquor can yield featureless topographs and mosaic widths comparable to those of unsoaked crystals. These results imply that the change in solution conditions does not introduce disorder measurable by topographs into the pre-change growth region.

A fourth possibility is that the equilibrium lattice constants corresponding to the pre- and post-change growth solutions are different, due to differences in molecular conformation, crystal contacts or solvent and small-molecule content. After the change, the pre-change growth region may gradually relax toward the new equilibrium lattice constant. Initial growth layers may attempt to grow with the new lattice constant onto only partially relaxed underlying layers, and the lattice constant mismatch may produce disorder. As the pre-change growth region relaxes, its volume will shrink or grow, and this may cause additional disordering of the post-change growth layers, particularly if the relaxation is nonuniform. Once the relaxation is complete, subse-

quent growth layers should become more ordered, but dislocations formed in the early growth regions may continue to propagate outward. Many of the features observed in the topographs of nonuniform growth crystals are consistent with this mechanism.

Lattice constant variations – such as those which occur when one material is grown epitaxically onto a second material having a different lattice constant [*e.g.*, GaAs on Si (Tiller, 1991)], when some materials are intercalated with small atoms or molecules, when the lattice undergoes a structural transformation [*e.g.*, martensitic transformations in steels (Barrett & Massalski, 1966)], or when adjacent materials have different thermal expansion coefficients – are an important source of disorder in inorganic materials. In all of these cases, lattice constant differences of as little as 0.1% are sufficient to produce substantial disorder. Many experiments provide evidence for variations in protein crystal lattice constants with solution conditions. Using the data of Salunke *et al.* (1985) for the unit-cell volume of tetragonal lysozyme as a function of humidity, and assuming that a saturated NaCl solution gives a humidity of 74% (Rockland, 1960), the ~0.8 *M* change in salt concentration experienced during growth by the crystals of Figs. 5, 6 and 12 corresponds to a humidity change of ~3.3%, a unit-cell volume change of roughly 0.7%, and a lattice constant change of roughly 0.2%. This suggests that the pre-change growth region of the crystal in Fig. 12 shrank by roughly 0.8 μm after the change in solution conditions. These magnitudes make plausible the notion that lattice constant variations during growth may contribute to the observed disorder.

4.3. *Implications for crystal growth practice*

The present results provide clear evidence that variations in solution conditions during growth can produce disorder in lysozyme crystals. The solution variations found to give the largest effects are more drastic than is typical of standard growth methods. However, even small changes, when performed abruptly, produce measurable disorder, and other proteins may be much more sensitive to solution conditions than lysozyme.

One obvious implication of these results is that macroseeding will create disorder. The amount of disorder should be reduced by matching the initial and final growth solutions. If a change in solution conditions to achieve more favorable growth conditions is desired, this change should be made gradually by, *e.g.* vapor diffusion. Another obvious implication is that precipitation and/or excessive nucleation that often occurs in the later stages of vapor diffusion and in other growth methods may introduce significant disorder, including dislocations that may substantially broaden crystal mosaicity.

Whether solution variations typical of vapor diffusion and other widely used growth techniques introduce enough disorder to appreciably affect the diffraction resolution will depend upon many factors. These include (1) the magnitude of the overall change in conditions; (2) the time for the change; (3) the sensitivity of growth kinetics and solubility to solution conditions (which will depend upon solution purity); (4) the sensitivity of the molecular conformation and lattice constant to solution conditions; (5) the time required for lattice relaxation in response to a change in conditions; (6) the extent to which the lattice is able to relax smoothly between different equilibrium lattice constants without trapping in metastable configurations; and (7) the background level of disorder arising from other mechanisms. These factors may vary considerably from protein to protein, and only further experimentation can reveal how often they conspire unfavorably.

5. Conclusions

X-ray topography and mosaicity measurements have established that solution variations during growth can result in substantial disorder in lysozyme crystals. Solution variations may generate disorder by producing transient changes in growth kinetics that favor defect-forming instabilities, by producing phase-separated droplets and precipitates that generate inclusions, and by producing changes in equilibrium molecular conformation and lattice constant. The experimental procedures described here should be broadly useful as diagnostics of protein crystal perfection and growth.

We wish to thank B. Batterman, J. Brock, C. Caylor, N. Campobasso, R. Collela, S. Ealick, R. Maimon, E. Siggia, J. Sethna, E. Snell, W. Wang, W. Webb and M. Weissman for fruitful discussions. This work was supported by NASA (NAG8-1357), with early support provided by the NSF (DMR-9424572).

References

Barrett, C. S. & Massalski, T. B. (1966). *Structure of Metals*. New York: McGraw Hill.

Cacioppo, E. & Pusey, M. L. (1991). *J. Cryst. Growth*, **114**, 286–292.

Chayen, N. E., Boggon, T. J., Cassetta, A., Deacon, A, Gleichmann, T., Habash, J., Harrop, S. J., Helliwell, J. R., Nieh, Y. P., Peterson, M. R., Raftery, J., Snell, E. H., Hadener, A., Niemann, A. C., Siddons, D. P., Stojanoff, V., Thompson, A. W., Ursby, T. & Wulff, M. (1996). *Quart. Rev. Biophys.* **29**, 227–278.

Chernov, A. A. (1997). *Phys. Rep.* **288**, 61–75.

Chernov, A. A. & Komatsu, H. (1995). *Science and Technology of Crystal Growth*, edited by J. P. van der Eerden & O. S. L. Bruinsma. Dordrecht: Kluwer Academic Publishers.

Cloetens, P., Barrett, R., Baruchel, J., Guigay, J.-P. & Schlenker, M. (1996). *J. Phys. D Appl. Phys.* **29**, 133–146.
Ducruix, A. & Giegé, R. (1992). *Crystallization of Nucleic Acids and Proteins*. Oxford: IRL Press.
Durbin, S. D. & Carlson, W. E. (1992). *J. Cryst. Growth*, **122**, 71–79.
Durbin, S. D., Carlson, W. E. & Saros, M. T. (1993). *J. Phys. D*, **26**, B128–B132.
Durbin, S. D. & Feher, G. (1990). *J. Mol. Biol.* **212**, 763–774.
Durbin, S. D. & Feher, G. (1996). *Ann. Rev. Phys. Chem.* **44**, 171–204.
Elgersma, A. V., Ataka, M. & Katsura, T. (1992). *J. Cryst. Growth*, **122**, 31–40.
Fourme, R., Ducruix, A., Riès-Kautt, M. & Capelle, B. (1995). *J. Synchrotron Rad.* **2**, 136–142.
Helliwell, J. R. (1988). *J. Cryst. Growth*, **90**, 259–272.
Izumi, K., Sawamura, S. & Ataka, M. (1996). *J. Cryst. Growth*, **168**, 106–111.
Klapper, H. (1980). In *Characterization of Crystal Growth Defects by X-ray Methods*, edited by B. K. Tanner & D. K. Bowen, pp. 133–160. New York: Plenum Press.
Konnert, J. H., D'Antonio, P. & Ward, K. B. (1994). *Acta Cryst.* D**50**, 603–613.
Koz'ma, A. A., Arinkin, A. V., Mikhaylov, I. F. & Fuks, M. Ya. (1973). *Fiz. Metal. Metalloved.* **36**, 596–604. (*Phys. Metals Metallogr.* **38**, 132–140).
Krivoglaz, M. A. (1996). *X-ray and Neutron Diffraction in Nonideal Crystals*. Berlin: Springer.
Kuznetsov, Yu. G., Malkin, A. J., Greenwood, A. & McPherson, A. J. (1995). *J. Struct. Biol.* **14**, 184–196.
Lin, H., Rosenberger, F., Alexander, J. I. D. & Nadarajah, A. (1995). *J. Cryst. Growth*, **151**, 153–62.
Long, G. (1998). Private communication.
McPherson, A., Malkin, A. J. & Kuznetsov, Yu. G. (1996). *Structure*, **3**, 759–768.
McPherson, A., Malkin, A. J., Kuznetsov, Yu. G. & Koszelak, S. (1996). *J. Cryst. Growth*, **168**, 74–92.
Maimon, R. (1997). Personal communication.
Malkin, A. J., Kuznetsov, Yu. G., Land, T. A., DeYoreo, J. J. & McPherson, A. (1995). *Nature Struct. Biol.* **2**, 956–959.
Metzger, T. H., Peisl, J. & Kaufmann, R. (1983). *J. Phys. F*, **13**, 1103–1113.
Monaco, L. A. & Rosenberger, F. (1993). *J. Cryst. Growth*, **129**, 465–484.
Muschol, M. & Rosenberger, F. (1997). *J. Chem. Phys.* **107**, 1953–1962.
Newkirk, J. B. & Wernick, J. H. (1962). *Imperfections in Crystals*. New York: Interscience.
Otalora, F., Capelle, B., Ducruix, A. & Garcia-Ruiz, J. M. (1997). Unpublished work.
Pusey, M., Witherow, W. K. & Naumann, R. (1988). *J. Cryst. Growth*, **90**, 105–111.
Rockland, L. B. (1960). *Anal. Chem.* **32**, 1375–1376.
Rodeau, J. L., Mikol, V., Giegé, R. & Lutun, P. (1991). *J. Appl. Cryst.* **24**, 135–141.
Rosenberger, F., Vekilov, P. G., Muschol, M. & Thomas, B. R., (1996). *J. Cryst. Growth*, **168**, 1–27.
Salunke, D. M., Veerapandian, B., Kodandapani, R. & Vijayan, M. (1985). *Acta Cryst.* B**41**, 431–436.
Shaikevitch, A. & Kam, Z. (1981). *Acta Cryst.* A**37**, 871–875.
Snell, E. H. (1997). Unpublished work.
Snell, E. H., Weisgerber, S., Helliwell, J. R., Weckert, E., Holzer, K. & Schroer, K. (1995). *Acta Cryst.* D**51**, 1099–1102.
Stojanoff, V. & Siddons, D. P. (1996). *Acta Cryst.* A**52**, 498–499.
Stojanoff, V., Siddons, D. P., Monaco, L. A., Vekilov, P. & Rosenberger, F. (1997). *Acta Cryst.* D**53**, 588–595.
Tanner, B. K. (1976). *X-ray Diffraction Topography*. Oxford: Pergamon Press.
Tanner, B. K. & Bowen, D. K. (1980). Editors. *Characterization of Crystal Growth Defects by X-ray Methods*. New York: Plenum Press.
Thomas, B. R., Vekilov, P. G. & Rosenberger, F. (1996). *Acta Cryst.* D**52**, 776–784.
Tiller, W. A. (1991). *The Science of Crystallization*. Cambridge University Press.
Vekilov, P. G., Alexander, J. I. D. & Rosenberger, F. (1996). *Phys. Rev. E*, **54**, 6650–6660.
Vekilov, P. G., Ataka, M. & Katsura, T. (1995). *Acta Cryst.* D**51**, 207–219.
Vekilov, P. G., Monaco, L. A., Thomas, B. R., Stojanoff, V. & Rosenberger, F. (1996). *Acta Cryst.* D**52**, 785–798.
Webb, W. W. (1962). *J. Appl. Phys.* **33**, 3546–3552.
Yip, C. M. & Ward, M. D. (1996). *Biophys. J.* **71**, 1071–1078.